Analytical continuation from bound to resonant states in the Dirac equation with quadrupole-deformed potentials

Xu-Dong Xu, Shi-Sheng Zhang, A. J. Signoracci, M. S. Smith, and Z. P. Li

Phys. Rev. C **92**, 024324 — Published 28 August 2015

DOI: 10.1103/PhysRevC.92.024324

Analytical continuation from bound to resonant states in the Dirac equation with quadrupole-deformed potentials

Xu-Dong Xu,[1] Shi-Sheng Zhang,[1,2,3,4,*] A. J. Signoracci,[3] M. S. Smith,[3,†] and Z. P. Li[5,‡]

[1]*School of Physics and Nuclear Energy Engineering, Beihang University, Beijing 100191, China*
[2]*Institute of Theoretical Physics, Chinese Academy of Sciences, Beijing 100190, China*
[3]*Physics Division, Oak Ridge National Laboratory, Oak Ridge, Tennessee, 37831-6354, USA*
[4]*Department of Physics and Astronomy, University of Tennessee, Knoxville, Tennessee, 37996, USA*
[5]*School of Physical Science and Technology, Southwest University, Chongqing 400715, China*

Background Resonances with pronounced single particle characteristics are crucial for quantitative descriptions of exotic nuclei near and beyond the drip lines, and often impact halo formation and nucleon decay processes. Since the majority of nuclei are deformed, the interplay between deformation and orbtial structure near threshold can lead to improved descriptions of exotic nuclei.

Purpose Develop a method to study single particle resonant orbital structure in the Dirac equation with a quadrupole-deformed Woods-Saxon potential. Determine the structure evolution of bound and resonant levels with deformation in this scheme, and examine the impact on halo formation in loosely bound systems, with a focus on the recent halo candidate nucleus ^{37}Mg.

Method Analytical continuation of the coupling constant (ACCC) method is developed on the basis of the Dirac equation with a deformed Woods-Saxon potential. The scalar and vector terms in the deformed potential are determined by the energies of the valence neutron and nearby orbitals, which are extracted from a self-consistent relativistic Hartree-Bogoliubov (RHB) calculation with the PC-PK1 density functional.

Results We compare the energies and widths of resonant orbitals in the recent halo nucleus candidate ^{37}Mg using the ACCC method based on the Dirac coupled-channel equations with those determined from the scattering phase shift (SPS) method. It is found that the results from the two methods agree well for narrow resonances, whereas the SPS method fails for broad resonances. Nilsson levels for bound and resonant orbitals from the ACCC method are calculated over a wide range of deformations and show some decisive hints of halo formation in ^{37}Mg.

Conclusions In our ACCC model for deformed potentials in the coupled-channel Dirac equations, the crossing of the configuration 1/2[321] and 5/2[312] orbitals at a deformation of approximately 0.5 enhances the probability to occupy the 1/2[321] orbital coming from $2p_{3/2}$ thereby explaining the recent observation of a p-wave one-neutron halo configuration in ^{37}Mg. The resonant 1/2[301] configuration plays a crucial role in halo formation in the magnesium isotopes beyond $A = 40$ for a wide range of deformations larger than 0.2.

PACS numbers: 21.10.Gv, 21.10.Pc, 21.60.Jz, 24.10.Eq

I. INTRODUCTION

The properties of nuclei far from stability are the focus of intense experimental and theoretical study [1–3]. Since the majority of nuclei close to the drip line are deformed, interplay between deformation and near-threshold orbitals can lead to new phenomena as shell structure evolves with deformation. For stable nuclei, most studies focus on the structure evolution of bound states. For drip-line nuclei, more factors need to be taken into account, since deformation readily changes the structure of low-lying positive-energy resonant orbitals, as well as the coupling of resonant and loosely-bound orbitals. The relevant resonances usually have a pronounced single particle (s.p.) nature due to their small binding energies; this leads to their important role in the formation of halo structure when pairing is taken into account [4]. For those nuclei beyond the drip line, nucleon decay processes are primarily determined by the nucleon decay widths of unbound s.p. resonances, which are dramatically altered with deformation. For these reasons, s.p. resonances in deformed nuclei are of great interest, and the determination of their energies, widths, and wavefunctions will be helpful in the search for halo candidates and new decay states.

There have been significant theoretical efforts to study resonant states in exotic nuclei [5–19]. Because of the numerical difficulties to solve the coupled-channel Schrödinger equations for deformed potentials, several non-self-consistent techniques have been used to obtain the energies and widths for s.p. resonant orbitals within this framework. The potential separable extension (PSE) approach [5] is one such technique, but has proven difficult for proton s.p. resonances. In Ref. [6], first order differential equations were integrated, instead of the second order coupled-channel Schrödinger equations, and applied to analyze neutron s.p. bound and resonant orbitals spectra with variable deformation. The analytical

*Electronic address: zss76@buaa.edu.cn
†Electronic address: smithms@ornl.gov
‡Electronic address: zpliphy@swu.edu.cn

continuation of the coupling constant (ACCC) method was combined with the Schrödinger equation to provide s.p. resonance parameters and then applied to proton decay [8]. The contour deformation method (CDM) [11] was applied to the momentum-space Schrödinger equation to study resonances in deformed mean-fields [13]. The scattering phase shift (SPS) method was employed to extract resonance parameters from the coupled-channel Schrödinger equations to study deformed cases with axially-deformed Woods-Saxon potentials [10]. It is, however, well known that the SPS method is applicable for narrow resonances but not for broad ones. Some resonances will be absent or disappear with deformation at finite energies in this approach [20] because eigenphases do not pass through $\pi/2$ when s- or p-wave components are mixed in [16]. The complex scaling (CS) method has been used to calculate resonance parameters for an axial-deformed potential in Ref. [18]. As mentioned in Ref. [21], back rotation in CS method can introduce large errors so that low-energy s.p. resonances near the threshold might not be found [18]; Padé approximants must be used for better accuracy for narrow resonances. Since the spin-orbit coupling interaction can be automatically included in the coupled-channel Dirac equations, the SPS [16] and CS method [22] have been recently developed within this framework for quadrupole-deformed potentials.

We aim at developing a self-consistent microscopic method to describe deformed nuclei including spin-orbital coupling, resonant contributions, and pairing correlations. For spherical nuclei, such a method has already been developed and used to describe Ni [23], Sn [24], Zr [25], and Ne isotopes [4, 26]. This work represents the first attempt to extend this method to deformed nuclei within the relativistic framework.

In this paper, we first present the formalism and numerical details to solve for bound states in the coupled-channel Dirac equations in coordinate space using a quadrupole-deformed Woods-Saxon potential. We then combine this with the ACCC method in order to extract energies and widths of neutron s.p. resonant orbitals. We then calculate, within our microscopic approach, the evolution of structure as a function of deformation for the recent p-wave halo candidate nucleus ^{37}Mg [27].

II. THEORETIAL FRAMEWORK

The Dirac equation with a quadrupole-deformed potential takes the form,

$$\Big\{\boldsymbol{\alpha}\cdot\boldsymbol{p} \;+\; \gamma_0\big[M+S_0(r)+S_2(r)Y_{20}(\theta,\phi)\big]+V_0(r) \;+\; V_2(r)Y_{20}(\theta,\phi)\Big\}\Psi_\Omega=\varepsilon_\Omega\Psi_\Omega, \tag{1}$$

where $S_0(r)+S_2(r)Y_{20}(\theta,\phi)$ and $V_0(r)+V_2(r)Y_{20}(\theta,\phi)$ represent the scalar and vector potentials in relativistic mean-field (RMF) theory, respectively [2]. The potentials $S_0(r)$ and $V_0(r)$ are the spherical terms, while $S_2(r)Y_{20}(\theta,\phi)$ and $V_2(r)Y_{20}(\theta,\phi)$ are the quadrupole terms. For simplicity, the higher-order multipole deformations are neglected. As in our previous work [16], the deformed Woods-Saxon form is used for the potentials $S_0(r)$, $S_2(r)$, $V_0(r)$, and $V_2(r)$.

The single-particle wave function with the parity and angular momentum z-component Ω as good quantum numbers can be expanded in terms of spherical Dirac spinors,

$$\Psi_\Omega=\sum_{lj}\begin{pmatrix} i\frac{G^{lj}_\Omega(r)}{r} \\ \frac{F^{lj}_\Omega(r)}{r}\sigma\cdot\hat{\mathbf{r}}\end{pmatrix}Y^l_{j\Omega}(\theta,\phi), \tag{2}$$

where $G^{lj}_\Omega(r)/r$ and $F^{lj}_\Omega(r)/r$ are respectively the radial wave functions for the upper and lower components, and $Y^l_{j\Omega}(\theta,\phi)$ are the spinor spherical harmonics. Then Eq. (1) can be reduced to the coupled-channel Dirac equations for the radial wave functions,

$$\frac{\mathrm{d}G^{lj}_\Omega}{\mathrm{d}r} \;+\; \frac{\kappa}{r}G^{lj}_\Omega-(\varepsilon_\Omega+M+V_0-S_0)F^{lj}_\Omega \;+\; \sum_{l'j'}(V_2-S_2)A(2,l'j',lj,\Omega)F^{l'j'}_\Omega=0, \tag{3}$$

$$\frac{\mathrm{d}F^{lj}_\Omega}{\mathrm{d}r} \;-\; \frac{\kappa}{r}F^{lj}_\Omega+(\varepsilon_\Omega-M-V_0-S_0)G^{lj}_\Omega \;-\; \sum_{l'j'}(V_2+S_2)A(2,l'j',lj,\Omega)G^{l'j'}_\Omega=0, \tag{4}$$

where $\kappa=(-1)^{j+l+1/2}(j+1/2)$ and $A(2,l'j',lj,\Omega)$ has the form,

$$A(2,l'j',lj,\Omega)=(-1)^{1/2+\Omega}\sqrt{\frac{(2j+1)(2j'+1)}{4\pi}}\begin{pmatrix} j & 2 & j' \\ -\Omega & 0 & \Omega\end{pmatrix}\begin{pmatrix} j' & 2 & j \\ \frac{1}{2} & 0 & -\frac{1}{2}\end{pmatrix} \tag{5}$$

The bound states can be obtained by solving these coupled equations in coordinate space with boundary condition $G^{lj}_\Omega(r)=0$ at $r=0$ and $r\to\infty$.

The resonant states will be studied with the ACCC method. The basic idea of this approach is that, for an attractive potential, a resonant state will become bound as the coupling constant λ (*i.e.*, the potential strength) is increased. In this scheme, it has been demonstrated that the wave number k is an analytic function of λ, with the same restrictions on the potential that guarantee the analyticity of the Jost function [28, 29]. Near the branch point λ_0, defined by the scattering threshold $k(\lambda_0)=0$, the wave number $k(\lambda)$ behaves as

$$k(\lambda)\sim\begin{cases} i\sqrt{\lambda-\lambda_0}, & l>0, \\ i(\lambda-\lambda_0), & l=0.\end{cases} \tag{6}$$

These properties demonstrate an analytic continuation of the wave number k in the complex plane from the

bound-state region into the resonance region by a Padé approximant of the second kind (PAII)

$$k(x) \approx k^{[L,N]}(x) = i\frac{c_0 + c_1 x + c_2 x^2 + \cdots + c_L x^L}{1 + d_1 x + d_2 x^2 + \cdots + d_N x^N} \quad (7)$$

where $x = \sqrt{\lambda - \lambda_0}$, and $c_0, c_1, \cdots, c_L, d_1, d_2, \cdots, d_N$ are the coefficients of PAII. These coefficients can be determined by a fit to a set of reference points $\{x_i, k(x_i)\}$ obtained from the Dirac equation with $\lambda_i > \lambda_0$, $i = 1, 2, \cdots, L + N + 1$. With the complex wave number $k(\lambda = 1) = k_r + ik_i$, the resonance energy E and the width Γ can be extracted from the relation $\varepsilon = E - i\Gamma/2$ and $k^2 = \varepsilon^2 - M^2$.

III. NUMERICAL DETAILS, RESULTS, AND DISCUSSION

The parameters for the Woods-Saxon potential are set as follows. The radius $R = 3.705$ fm is taken from a self-consistent spherical relativistic Hartree-Bogoliubov (RHB) calculation with the PC-PK1 density functional [30] for ^{37}Mg. The depth for the scalar and vector potentials $S_{\rm WS} = -420.3$ MeV and $V_{\rm WS} = 349.7$ MeV are determined by reproducing the energy of the last bound state $1f_{7/2}$ and the energy difference between $1d_{3/2}$ and $1d_{5/2}$ obtained by the RHB calculation. Finally, the diffuseness of the potential a is fixed as 0.67 fm. The coupled equations (3, 4) are solved in r space with a mesh step 0.1 fm and a cutoff at $R_{\rm box} = 20$ fm which is sufficiently large for convergence. For the state with Ω^π, 8 channels with $j \geqslant \Omega$ and $(-1)^l = \pi$ are considered in Eq. (2). The Padé approximant in Eq. (7) converges for orders $L = N = 4$ and above, as demonstrated for the spherical case [9]. It is noted that the coupling constant λ should be multiplied to the spherical portion (i.e., $V_0 + S_0$ in Eq. (4)) of the attractive potential. This is important to maintain a smooth continuation of the level energy as a function of deformation parameter β for any resonant orbital.

All the levels are labeled by the asymptotic Nilsson quantum numbers $\Omega[Nn_z\Lambda]$, in which Ω is the projection of the single particle total angular momentum onto the z axis, N is the principal quantum number, n_z is the number of nodes of the wave function in the z direction, and Λ is the projection of the orbital angular momentum l onto the z axis. Figure 1 displays the resonance energy E and width Γ for the neutron resonant state 3/2[301] as functions of the coupling constant λ in the quadrupole-deformed Woods-Saxon potential with $\beta = 0.47$ as an example. A newly developed microscopic self-consistent approach, a deformed relativistic Hartree theory in a spherical Woods-Saxon basis (DRHSWS) [31] suggests this approximate deformation for ^{37}Mg with NL3 [32] effective interaction. Filled circles are the solutions of the Dirac equation, which are used to determine the coefficients in the PAII approximant (solid line). This PAII polynomial fit is then extrapolated to larger λ values

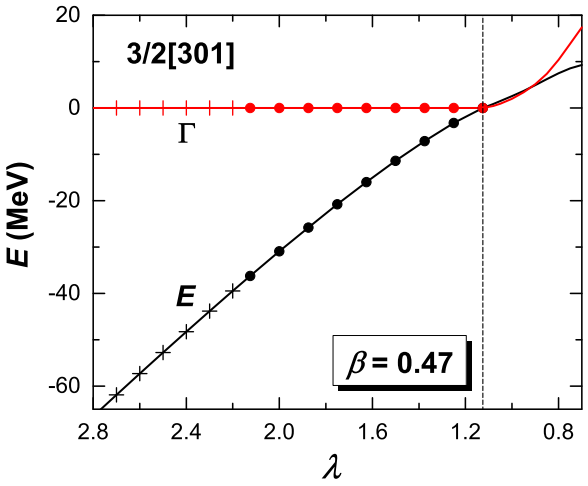

Fig. 1: (color online) Energy E and width Γ of the neutron resonant state 3/2[301] as functions of the coupling constant λ in the quadrupole-deformed Woods-Saxon potential with $\beta = 0.47$. Filled circles and crosses are the solutions of the Dirac equation, and the former is used as input in the ACCC method. Solid curves are the outcome of the Padé approximant with $L = N = 4$ for energy (black) and width (red).

where it compares well to discrete values (exact solutions) shown by cross marks in Fig. 1. The smoothness of the solid lines indicates good analyticity of the eigenvalues for the Dirac equation with respect to the coupling constant. The dashed vertical line indicates the branch point $\lambda_0 = 1.125$ where the orbital energy becomes zero. As λ continues to decrease from λ_0 down to 1, a nonvanishing imaginary part appears in the complex energy. At $\lambda = 1$, one obtains the resonance energy E and width Γ for the 3/2[301] orbital.

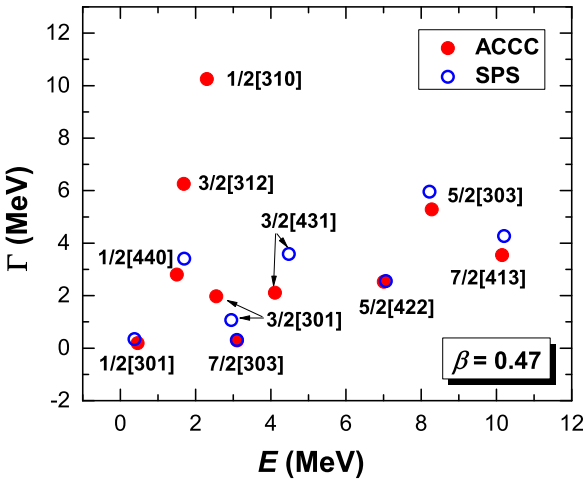

Fig. 2: (color online) Energies and widths of the neutron resonant states for the quadrupole-deformed Woods-Saxon potential with $\beta = 0.47$. Solid circles represent the results of the ACCC method, while open circles denote the results of SPS method.

In Fig. 2, we compare the energies and widths for 10 low-lying resonant states calculated by the ACCC method with those obtained from the SPS method [16] in the quadrupole-deformed Woods-Saxon potential with $\beta = 0.47$. The SPS method, which is a more direct approach, has been demonstrated to work well with deformed orbitals that have narrow widths [16]. Fig. 2 shows good agreement of the ACCC results with those from the SPS method for many states. The agreement worsens for broad resonant states with $E \leqslant \Gamma$. And the SPS method eventually fails at widths greater than 6 MeV, which is due to the large mixing of the low l (s- or p-wave) components [16].

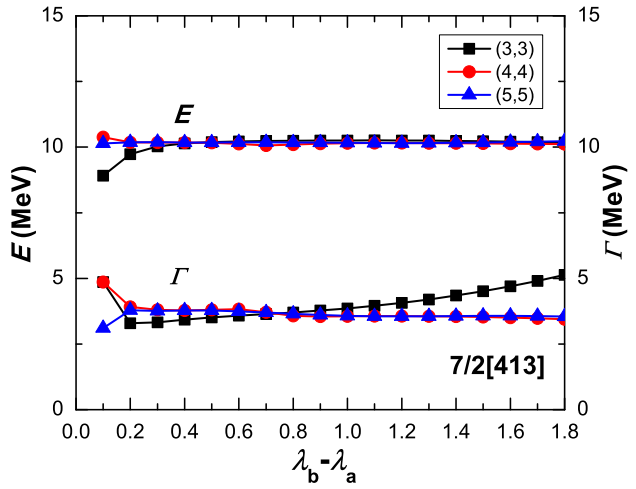

Fig. 3: (color online) Energies and widths of the neutron resonant state 7/2[413] as a function of increasing length of the λ_i values interval $[\lambda_a, \lambda_b]$ for Padé approximant orders $L = N = 3$ (black solid squares lines), 4 (red solid circles lines), and 5 (blue solid triangles lines). These are carried out for a quadrupole-deformed Woods-Saxon potential with $\beta = 0.47$.

Figure 3 displays the convergence of the energies and widths of the neutron resonant state 7/2[413] with the Padé approximant of orders $L = N = 3, 4, 5$ in Eq. (7). It also shows the stability of the Padé approximant as the length of the λ_i values interval $[\lambda_a, \lambda_b]$ increases. Here λ_a and λ_b have the same meaning as those specified in Ref. [9]. As can be seen in Fig. 3, convergence occurs with a PAII order of $L = N = 4$ and above; stability of the PAII is also shown to be valid when the length of $[\lambda_a, \lambda_b]$ is sufficiently large. From this example, we conclude that the ACCC method enables us to study broad resonant states with higher energies ($E \geqslant 5.0$ MeV) and higher angular momentum ($l \geqslant 2$) while fulfilling both convergence and stability.

Figure 4 presents the evolution of the single-neutron levels, including both bound and resonant states, as functions of β in quadrupole-deformed Woods-Saxon potential. In the spherical case, the calculated energy difference between the bound $1f_{7/2}$ level and the very low-

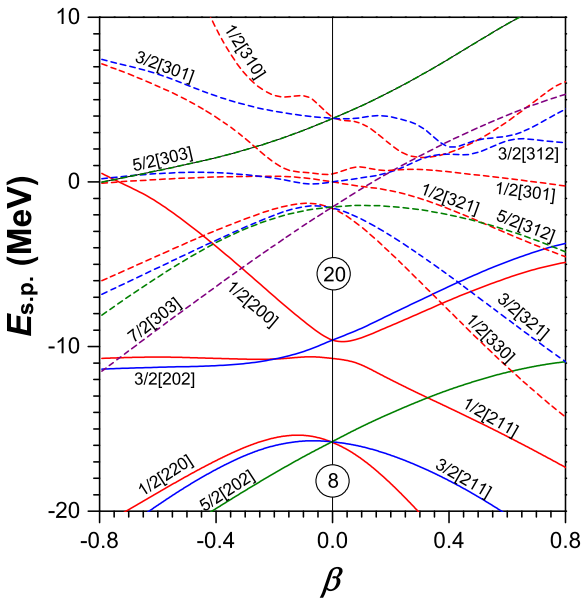

Fig. 4: (color online) The single-neutron levels as a function of β in a quadrupole-deformed Woods-Saxon potential whose parameters are determined by the self-consistent RHB calculation for ^{37}Mg. All the levels are labeled by the asymptotic Nilsson quantum numbers $\Omega[Nn_z\Lambda]$.

lying one-particle resonant state $2p_{3/2}$ is only ~ 1.5 MeV, which clearly indicates that the $N = 28$ energy gap at $\beta = 0$ disappears in neutron rich Mg isotopes. This is consistent with our systematic calculations on $N = 28$ isotones by the triaxial relativistic Hartree-Bogoliubov model with DD-PC1 density functional [33]. A pronounced deformed shell gap at $\beta \sim 0.45$ is observed, which corresponds to the neutron number $N = 24$. This drives a prolate minimum in the nuclei around ^{37}Mg [34, 35]. Of particular interest is the behavior of the 1/2[321] state, which drops to energies below those of the 5/2[312] state around the deformed shell gap. This results in an enhanced probability to occupy the 1/2[321] orbital, providing an explanation for the recent observation [27] of a p-wave one-neutron halo configuration in ^{37}Mg. A similar patten of single-neutron levels was predicted by Hamamoto in Ref. [36], but in that study the 1/2[301] orbital was not obtained as a single-particle resonant state, and the resonant 1/2[310] and 3/2[301] orbitals disappear for larger deformation. Similar to Refs. [31, 35], the resonant 1/2[301] orbital lies close to the threshold and therefore likely plays a crucial role in halo formation in the magnesium isotopes beyond $A = 40$ for a wide range of deformations larger than 0.2. The Nilsson diagram for ^{40}Mg is quite similar to that for ^{37}Mg shown in Fig. 4. Additional studies are needed to determine the mutual impact of deformation, pairing correlations, and resonant state contributions on halo formation and structure evolution for deformed Mg isotopes.

As an independent confirmation of our predicted configuration 1/2[321] coming from $2p_{3/2}$ orbital for

well-deformed ^{37}Mg, we performed a large-scale shell model (SM) calculation for ^{37}Mg with the code NUSHELLX@MSU [37] using the SDPF-U [38] effective interaction. To reduce the computational cost, we assumed that the protons occupy only *sd* orbits, the $1d_{5/2}$ neutron orbital is fully occupied, and the $1f_{5/2}$ neutron orbital is unoccupied. We obtained a ground state $J^\pi = 1/2^-$, primarily composed of four protons in the $1d_{5/2}$ orbital. The neutron configuration essentially fills the *sd* orbitals and consists further of four neutrons in the $1f_{7/2}$ orbital, and one neutron in the $2p_{3/2}$ orbital as the primary configuration (40%). There is significant mixing with other configurations, most notably with two neutrons in the $2p_{3/2}$ orbital and three in the $1f_{7/2}$ orbital (25%). There is also a $J^\pi = 3/2^-$ state at 90 keV excitation energy, with a similar configuration to the ground state and $J^\pi = 5/2^-$ state at 406 keV. Our SM calculations are consistent with similar calculations [27] using the SDPF-M [39] effective interaction, and mostly confirm our conclusion according to the Nilsson diagram in Fig. 4.

IV. SUMMARY

We have developed a solution of the coupled-channel Dirac equations in coordinate space using a quadrupole-deformed Woods-Saxon potential. We combined this with the ACCC method to extract energies and widths of neutron s.p. resonant orbitals as a function of deformation. This is a first step towards developing a self-consistent microscopic method to describe deformed nuclei including spin-orbital coupling, resonant contributions, and pairing correlations within a relativistic framework. We have used our microscopic approach to calculate the evolution of structure as a function of deformation for the recent *p*-wave halo candidate nucleus ^{37}Mg, and find some decisive hints of halo formation at deformations of approximately 0.5. Our future efforts will be to use this approach, along with the RMF theory and BCS approximation for pairing, to quantitatively evaluate the contribution of resonances to the structure of ^{42}Mg, which may be a promising halo candidate in well-deformed Mg isotopes.

V. ACKNOWLEDGEMENT

We acknowledge Dr. G. Hagen for his careful reading of the manuscript. This work has been supported by the National Natural Science Foundation of China (Grants Nos. 11375022, 11235002, 11475140, and 11105110); China Scholarship Council (No. 2011307472), Beihang New Star; International Science and Technology Cooperation Projects (2012DFG61930); and the U.S. Dept. of Energy, Office of Nuclear Physics.

[1] I. Tanihata, H. Savajols, and R. Kanungod, Prog. Part. Nucl. Phys. **68**, 215 (2013).
[2] J. Meng and P. Ring, Phys. Rev. Lett. 77, 3963 (1996); J. Meng, H. Toki, S. G. Zhou, S. Q. Zhang, W. H. Long, and L. S. Geng, Prog. Part. Nucl. Phys. **57**, 470 (2006).
[3] J. Dobaczewski, W. Nazarewicz, T. R. Werner, J.-F. Berger, C. R. Chinn, and J. Dechargé, Phys. Rev. C **53**, 2809 (1996).
[4] S. S. Zhang, M. S. Smith, Z. S. Kang, and J. Zhao, Phys. Lett. B **730**, 30 (2014).
[5] Z. Papp, J. Phys. A **20**, 153 (1987).
[6] L. S. Ferreira, E. Maglione, and R. J. Liotta, Phys. Rev. Lett. **78**, 1640 (1997).
[7] A. T. Kruppa, P. H. Heenen, H. Flocard, and R. J. Liotta, Phys. Rev. Lett. **79**, 2217 (1997).
[8] G. Cattapan and E. Maglione, Phys. Rev. C **61**, 067301 (2000).
[9] S. S. Zhang, J. Meng, S. G. Zhou, and G. C. Hillhouse, Phys. Rev. C **70**, 034308 (2004).
[10] I. Hamamoto, Phys. Rev. C **69**, 041306 (2004).
[11] G. Hagen, J. S. Vaagen, and M. Hjorth-Jensen, J. Phys. A: Math. Gen. **37**, 8991 (2004).
[12] N. Michel, W. Nazarewicz, and M. Ploszajczak, Phys. Rev. C **70**, 064313 (2004).
[13] G. Hagen and J. S. Vaagen, Phys. Rev. C **73**, 034321 (2006).
[14] L. Zhang, S. G. Zhou, J. Meng, and E. G. Zhao, Phys. Rev. C **77**, 014312 (2008).
[15] H. Oba and M. Matsuo, Phys. Rev. C **80**, 024301 (2009).
[16] Z. P. Li, J. Meng, Y. Zhang, S. G. Zhou, and L. N. Savushkin, Phys. Rev. C **81**, 034311 (2010).
[17] Y. Zhang, M. Matsuo, and J. Meng, Phys. Rev. C **83**, 054301 (2011).
[18] Q. Liu, J. Y. Guo, Z. M. Niu, and S. W. Chen, Phys. Rev. C **86**, 054312 (2012).
[19] T. T. Sun, S. Q. Zhang, Y. Zhang, J. N. Hu, and J. Meng, Phys. Rev. C **90**, 054321 (2014).
[20] I. Hamamoto, Phys. Rev. C **72**, 024301 (2005).
[21] N. Michel, W. Nazarewicz, M. Ploszajczak, and T. Vertse, J. Phys. G **36**, 013101 (2009).
[22] M. Shi, Q. Liu, Z. M. Niu, and J. Y. Guo, Phys. Rev. C **90**, 034319 (2014).
[23] S. S. Zhang, Int. J. Mod. Phys. E **18**, 1761 (2009).
[24] S. S. Zhang, M. S. Smith, G. Arbanas, and R. L. Kozub, Phys. Rev. C **86**, 032802 (2012).
[25] S. S. Zhang, X. D. Xu, and J. P. Peng, Eur. Phys. J. A **48**, 40 (2012).
[26] S. S. Zhang, X. D. Xu, and J. P. Peng, Eur. Phys. J. A **49**, 77 (2013).
[27] N. Kobayashi *et al.*, Phys. Rev. Lett. **112**, 242501 (2014).
[28] V. I. Kukulin, V. M. Krasnopolśky, and M. Miselkhi, Sov. J. Nucl. Phys. **29**, 421 (1979).
[29] J. R. Taylor, *Scattering Theory* (Wiley, New York, 1972).
[30] P. W. Zhao, Z. P. Li, J. M. Yao, and J. Meng, Phys. Rev. C **82**, 054319 (2010).
[31] S. G. Zhou, J. Meng, P. Ring, and E. G. Zhao, Phys. Rev. C **82**, 011301(R) (2010).
[32] G. A. Lalazissis, J. Konig, P. Ring, Phys. Rev. C **55**, 540

(1997).
[33] Z. P. Li, J. M. Yao, D. Vretenar, T. Niksic, H. Chen, and J. Meng, Phys. Rev. C **84**, 054304 (2011).
[34] J. M. Yao, H. Mei, H. Chen, J. Meng, P. Ring, and D. Vretenar, Phys. Rev. C **83**, 014308 (2011).
[35] L. L. Li, J. Meng, P. Ring, E. G. Zhao, and S. G. Zhou, Phys. Rev. C **85**, 024312 (2012).
[36] I. Hamamoto, Phys. Rev. C **76**, 054319 (2007).
[37] NuShellX@MSU, B. A. Brown, W. D. M. Rae, E. McDonald and M. Horoi, http://www.nscl.msu.edu/~brown/resources/resources.html; NuShellX, W. D. M. Rae, http://www.garsington.eclipse.co.uk/.
[38] F. Nowacki and A. Poves, Phys. Rev. C **79**, 014310 (2009).
[39] Y. Utsuno, T. Otsuka, T. Mizusaki, and M. Honma, Phys. Rev. C **60**, 054315 (1999).